

# BRDF CORRECTION ON AVHRR IMAGERY FOR SPAIN

H. Heisig

Institut für Photogrammetrie und Fernerkundung, Universität Karlsruhe, D-76137 Karlsruhe heisig@ipf.uni-karlsruhe.de

## TS 3 YF Youth Forum - Remote Sensing

**KEY WORDS:** Remote Sensing, Radiometry, Correction, Model, Land Cover

### ABSTRACT

The free reception of Advanced Very High Resolution Radiometer (AVHRR) data keeps a growing interest for the remote sensing community concerned with vegetation studies on regional and global scales. However, the use of AVHRR data for long-term quantitative monitoring requires consistent surface reflectance data. This implies correcting the effects from varying sun sensor target geometries in multitemporal AVHRR data sets described by the Bidirectional Reflectance Distribution Function (BRDF). In a joint research undertaken by the Geography Department of the University of Alcalá (Spain) and the Canadian Centre for Remote Sensing (CCRS) a new semi-empirical model, the Non-linear Temporal Angular Model (NTAM), has been applied for the BRDF correction of AVHRR data for Spain. Reflectance data derived from AVHRR channels 1 and 2 were corrected for BRDF effects by normalization to a standard viewing geometry. The study period was between May and September 2002. The required correction parameters were derived by model inversion. In order to obtain a good representation of the temporal and spatial dimensions of the data to be corrected, a sampling scheme was implemented. The land cover based approach of the NTAM was accounted for by the use of CORINE Land Cover data from Spain. A cloud mask algorithm was used to exclude cloud contaminated observations in the sampling data. The evaluation of the statistical parameters obtained from model inversion showed good results for practically all land cover classes in the two channels. Derived parameters allow for visualization of angular dependence of reflectance for different land cover classes.

### 1. INTRODUCTION

Current research work at the Geography Department at the University of Alcalá is strongly focussed on the field of fire risk assessment (Chuvienco 2002). Since 1998 the department receives AVHRR data in the High Resolution Picture Transmission (HRPT) format through an own receiver. These data are used for estimation of plant water content with the purpose of incorporating these estimations in fire risk indices (Aguado et al., 2003; Chuvienco et al., 2003).

Sun-synchronous polar-orbiting satellites like the National Oceanic and Atmospheric Administration (NOAA) AVHRR sensors are operated on must have such an orbital inclination that the rate of the resulting precession compensates for the motion of the Earth around the sun (Cracknell 1997). The satellite's orbit tracks projected on the Earth's surface reveal a parallel shift of about one degree east per day. This results in changing view angles for the same target within consecutive day passes.

### BRDF

Vegetation, as most other surfaces, does not scatter irradiance in equal quantities in all directions. In fact, it shows a behaviour far from being Lambertian (Dymond et al., 2001). Its reflectance depends on the angle of observation as well as on the angle of the incidence of the solar radiation. This bi-directional dependency lead to the idea of the BRDF (Bidirectional Reflectance Distribution Function). The BRDF describes the ratio of radiance  $dL_r$  [ $W m^{-2} sr^{-1} nm^{-1}$ ] reflected in one direction ( $\theta_r, \phi_r$ ) to the irradiance  $dE_i$  [ $W m^{-2} nm^{-1}$ ] from direction ( $\theta_i, \phi_i$ ) (Sandmeier & Itten, 1999). Figure 1 displays the angles that the BRDF is dependent on.

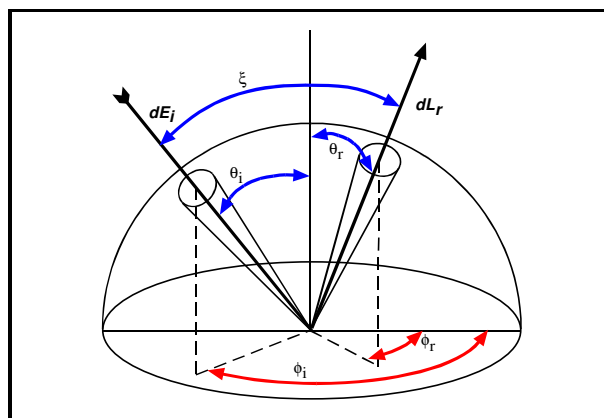


Figure 1: Concepts and parameters of the BRDF (Sandmeier & Itten, 1999, modified)

where:

$\theta_i$  = zenith incidence angle

$\theta_r$  = zenith reflection angle

$\phi_i$  = azimuth incident angle

$\phi_r$  = azimuth reflection angle

$\xi$  = phase angle

Parallel to the enhancement of BRDF measuring methods (goniometers, measurements from helicopters), considerable effort has been spent on development and testing of analytical and empirical models to describe the BRDF (Chen & Cihlar, 1997; Chopping, 2000; Hu et al., 1997; Ni et al., 1999; Ni & Li, 2000; O'Brien et al., 1998; Roujean et al., 1992; Wanner et al., 1995). BRDF models potentially allow for prediction of reflectance for any desired sun sensor target geometry.

Because partial cloud cover is practically always existent on a regional scale, different algorithms for creation of cloud-free AVHRR composites were developed. The composites are typically made from 10 day periods.

BRDF effects in AVHRR composite imagery can visually be noted through a non-coherent and coarse structure as well as striping effects. The normalization to a standard viewing geometry potentially reduces significantly such effects. In the case of correlation of different indices with field measured plant water contents it is assumed that BRDF corrected AVHRR imagery will yield better correlations and thus enhance the certainty of predictions.

## 2. METHODOLOGY

### 2.1 Data sets

In this study, AVHRR data from NOAA 15 and NOAA 16 covering part or the whole Iberian Peninsula were used. The daily NOAA 16 data acquisition time is between 3 and 4:30 pm, data from NOAA 15 are usually received between 9:30 and 11:00 am. The data is received in the HRPT format through a parabolic antenna. The data are calibrated as described by the NOAA manuals (KLM Users Guide, 2000). In order to avoid strong geometric and radiometric distortions, only data with a scan angle smaller than 45° were used. The image data are georeferenced and reprojected. The size of the imagery is 1136 by 889 pixels. The data sets used in this study were received between May and September 2002.

### 2.2 Models

The model applied for normalization of AVHRR data in this study is the NTAM (Non-linear Temporal Angular Model) as described by Latifovic et al. (2003). It is based on the widely used Roujean model (Roujean et al., 1992). The Roujean model and the empirical modified Walthall model (MWM, Walthall et al. 1985) are used for comparison of model performance. The three models are defined as follows:

The **Roujean model**:

$$\rho(\theta_i, \theta_r, \phi) = k_0 + k_1 f_1(\theta_i, \theta_r, \phi) + k_2 f_2(\theta_i, \theta_r, \phi)$$

The **modified Walthall model**:

$$\rho(\theta_i, \theta_r, \phi) = a_0(\theta_i^2 + \theta_r^2) + a_1\theta_i^2\theta_r^2 + a_2 \cos(\phi) + a_3$$

The **NTAM**:

$$\rho_i(\theta_i, \theta_r, \phi, \alpha_i) = \left[ 1 + a_{7,i}(j) e^{-\frac{\xi}{\pi} a_{8,i}(j)} \right] * \left[ 1 + (a_{1,i}(j) + a_{2,i}(j)(1 - \alpha_i) + a_{3,i}(j)(1 - \alpha_i)^2) f_1(\theta_i, \theta_r, \phi) + (a_{4,i}(j) + a_{5,i}(j)\alpha_i + a_{6,i}(j)\alpha_i^2) f_2(\theta_i, \theta_r, \phi) \right]$$

where:

$$f_1(\theta_i, \theta_r, \phi) = \frac{1}{2\pi} [(\pi - \phi) \cos \phi + \sin \phi] \tan \theta_i \tan \theta_r - \frac{1}{\pi} (\tan \theta_i + \tan \theta_r + \sqrt{\tan^2 \theta_i + \tan^2 \theta_r - 2 \tan \theta_i \tan \theta_r \cos \phi})$$

$$f_2(\theta_i, \theta_r, \phi) = \frac{4}{3\pi} * \frac{1}{\cos \theta_i + \cos \theta_r} \left[ \left( \frac{\pi}{2} - \xi \right) \cos \xi + \sin \xi \right] - \frac{1}{3}$$

$$\cos \xi = \cos \theta_i \cos \theta_r + \sin \theta_i \sin \theta_r \cos \phi$$

$$\alpha_i = \frac{\text{NIR} - \text{VIS}}{\text{NIR} + \text{VIS}} = \text{NDVI}$$

$$\alpha_2 = \text{NIR} - \text{VIS}$$

and:

$\rho$  = reflectance

$\phi$  = relative azimuth angle =  $|\phi_i - \phi_r|$

$j$  = land cover class

$i$  = AVHRR channel (1 = VIS, 2 = NIR)

The Roujean model belongs to the important group of physically based BRDF models that have reflectance as a linear function of parameters (Shepherd & Dymond, 2000). It considers the observed directional reflectance as the sum of a geometric and a volume scattering component. The parameters  $k_0$ ,  $k_1$  and  $k_2$  are semi-empirical coefficients representing physical properties of the surface. They are often referred to as 'kernels' (Wanner et al., 1995). In model inversion  $k_0$ ,  $k_1$  and  $k_2$  are obtained on a per-pixel base through least squares fit between model and observations by minimizing an error function.

Because the BRDF is time-wise dynamic, derivation of the model parameters in multitemporal data sets requires regression techniques made in subperiods (Leroy & Roujean, 1994). The number of cloud free observations within a sub period of about 10 days can thus easily become a limiting factor (Cihlar et al., 2002). The Modified Walthall model is a purely empirical model employing the four parameters  $a_0$ ,  $a_1$ ,  $a_2$  and  $a_3$ .

The NTAM was designed at the Canadian Centre of Remote Sensing (CCRS) for normalization of AVHRR imagery from northern ecosystems (Chen & Cihlar, 1997; Cihlar et al., 2002). The defined aim of this study is to investigate its applicability in a Mediterranean environment. The NTAM modifies the Roujean model to a time-independent, non-linear, physically based 8 parameter BRDF model. Model inversion is to be applied on land cover classes rather than on a per-pixel base. The temporal dimensions of the NTAM are approximated by polynomials that are related to vegetation indices. They account for the varying green leaf area during the growing season and the land cover dependent patterns of geometric and volume scattering components (Latifovic et al., 2003).

### 2.3 Cloud Mask Processing

For the generation of cloud free input sampling data a cloud detection algorithm based on the formulations of Saunders & Kriebel (1988) is applied. The algorithm consists of five tests that are applied to each individual pixel. A pixel is only considered to be cloud free if all the tests prove negative.

### 2.4 Spatial sampling

The NTAM requires a database that assigns each pixel in the imagery to a land cover class. In this study, CORINE Land Cover data from Spain are used to assign land cover class membership. CORINE Land Cover describes land cover based

on a nomenclature of 44 classes that are hierarchically organised into three levels (CORINE Land Cover Report, 2000). These data were reprojected to fit projection and cell size of the AVHRR imagery.

The original land cover types were aggregated into 14 land cover classes to represent major structural and surface cover combinations. For each aggregated land cover class between 60 and 100 sampling points were defined. Minimum distance to pixels of other classes was 5 pixels, minimizing thus the effect of transition pixels. For these sampling points the median reflectance value from a 3\*3 window were sampled. Table 1 lists the agglomerated CORINE Land Cover classes and their relative fraction of the surface of Spain.

Aggregated class	Comprises classes	% coverage
12	12: Non irrigated arable land	23.08
13	13: Irrigated arable land	7.53
	15: Vine yards	
	16: Fruit trees and berry plantations	
17	17: Olive grows	3.13
20	18: Pastures	8.39
	19: Annual with permanent crops	
	20: Complex cultivation patterns	
21	21: Agriculture with natural vegetation	5.23
22	22: Agro forestry areas	4.73
23	23: Broad leaved forests	6.88
24	24: Coniferous forests	9.00
25	25: Mixed forests	2.11
26	26: Natural grassland	5.54
27	27: Moors and heathland	3.54
28	28: Sclerophyllous vegetation	10.27
29	29: Transitional woodland shrub	6.45
31	31: Bare rock	2.42
	32: Sparsely vegetated areas	
0	All other classes (mainly settlements)	1.70

Table 1: CORINE Land Cover classes and relative fraction of surface

### 2.5 Temporal and angular sampling

Data were sampled from cloud mask processed datasets from throughout the study period. Between 1000 and 2000 observations per aggregated land cover class were obtained. Alternatively to cloud mask processing, data might have been sampled from cloud free composites.

### 2.6 Model inversion and statistic parameters

For model inversion, the CCRS kindly provided its MIB (Model Inversion of BRDF) software tool. For the linear models, the MIB works on a matrix inversion based procedure. For the NTAM, the modified Powell's minimization method is used to calculate the non-linear least squares fit in an iterative procedure (Latifovic et al., 2003). Statistic parameters used in the MIB are:

- The coefficient of determination  $R^2$  defined by:

$$R^2 = 1 - \frac{\delta^2}{\delta_{obs}^2}$$

where:

$$\delta^2 = \frac{1}{N} \sum_{i=1}^N [\rho_i - (\rho_{obs})_i]^2$$

$$\delta_{obs}^2 = \frac{1}{N} \sum_{i=1}^N (\rho_{obs})_i^2 - \left[ \frac{1}{N} \sum_{i=1}^N (\rho_{obs})_i \right]^2$$

- The standard error of the estimate (se) defined by:

$$se = \sqrt{\frac{\sum_{i=1}^N [\rho_i - (\rho_{obs})_i]^2}{N}}$$

where:

$\rho_{obs}$  = observed reflectance

$\rho$  = modelled reflectance

N = number of observations

## 3. RESULTS AND DISCUSSION

The CORINE Land Cover class 17 (olive grows), maybe the most emblematic land cover for Spain, was chosen to demonstrate the quality of the regression. In figure 2 modelled and observed reflectance are displayed for the sampling data in the NIR channel. 1052 observations were collected from NOAA 15 data and 852 observations originate from NOAA 16 data. The data from the two sensors were inverted together. They are displayed in different colours only for better legibility.

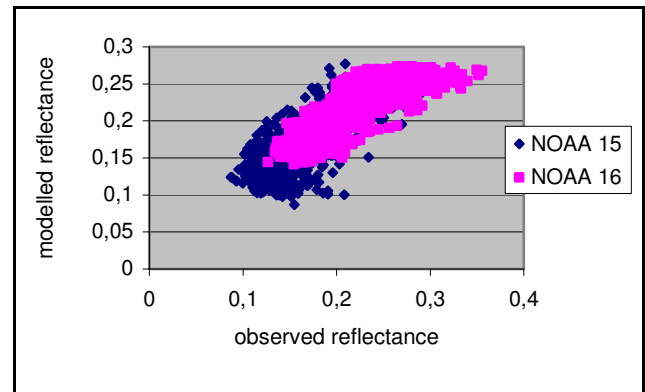


Figure 2: Observed and modelled reflectances for olive grows

The statistic results of the inverse mode are very satisfying. Figure 3 displays the coefficient of determination for the different aggregated land cover classes. The mean coefficient of determination for all land cover classes is 0.79 for the VIS and 0.83 for the NIR channel. Homogeneous land cover classes, e.g. class 17: olive grows and class 24: coniferous forest, are generally only slightly better modelled than more heterogeneous classes. For the latter ones, the classes 12, arable land, and 20, complex cultivation patterns may be named as examples. This shows well how the NTAM accounts for the varying amount of green leaf area within one vegetation class.

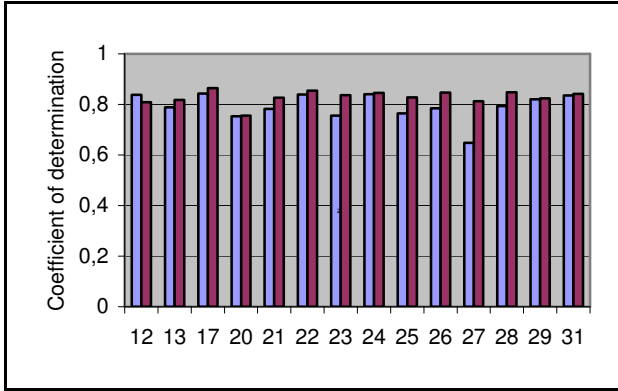


Figure 3: Coefficient of determination for the different aggregated land cover classes (left column= VIS, right column= NIR)

In order to investigate the regression quality of either NOAA 15 and NOAA 16 sampling data, corresponding data sets were separately introduced into the MIB. Mean values of the obtained statistical parameters for all classes and channels are displayed in table 2 and are compared between those obtained by running the MIB with the combined sampling data set.

Observations from	Channel	Avg $R^2$	Avg se
NOAA 15	VIS	0.804	0.015
	NIR	0.814	0.019
NOAA 16	VIS	0.870	0.016
	NIR	0.838	0.020
NOAA 15 & 16	VIS	0.792	0.018
	NIR	0.830	0.023

Table 2: Statistical results for model inversion for different input data sets

The input data sampling set that combines NOAA 15 and NOAA 16 observations was also introduced into the MIB in order to compare the performance with the Roujean and the Modified Walthall model. Table 3 displays the corresponding results. The NTAM yields best values for the coefficient of

determination, especially in the VIS channel. However, this is not too surprising as neither the Roujean model nor the MWM were designed to cope with sample data encompassing the entire growing season.

Model	Channel	Avg $R^2$	Avg se
Roujean	VIS	0.545	0.016
	NIR	0.729	0.025
Modified Walthall	VIS	0.535	0.016
	NIR	0.721	0.024
NTAM	VIS	0.792	0.018
	NIR	0.830	0.023

Table 3: Statistical results for model inversion for the three different models

Another very interesting extension from the determination of the correction parameters consists in a graphical visualization of modelled reflectances for different sun sensor target geometries (Sandmeier & Itten 1999, Dymond et al. 2001). Again, the land cover class 17 (olive grows) is chosen for such a visualization. As NTAM modelled reflectances depend on values for the proxies  $\alpha_i$ , a criterion had to be established that allows to display modelled reflectances for land cover typical  $\alpha_i$  values: First, the mean  $\alpha_i$  value of the input sampling data was calculated for the two channels. Then, the corresponding standard deviation values were added and subtracted from the mean  $\alpha_i$  values. The figures 4 to 7 show modelled reflectances for the VIS and the NIR. The raa is the relative azimuth angle, the vza the view zenith angle and the sza is the sun zenith angle. The sza is set to the fixed value of 45 degrees in all graphics. Note that no input data with a vza > 45° are introduced. Modelling to a vza of 52.5° is done to demonstrate model behaviour outside the range of calibration. The displayed graphics allow to estimate seasonal and angular dependency of the BRDF on different land covers. The hot spot is clearly distinguishable in all graphics.

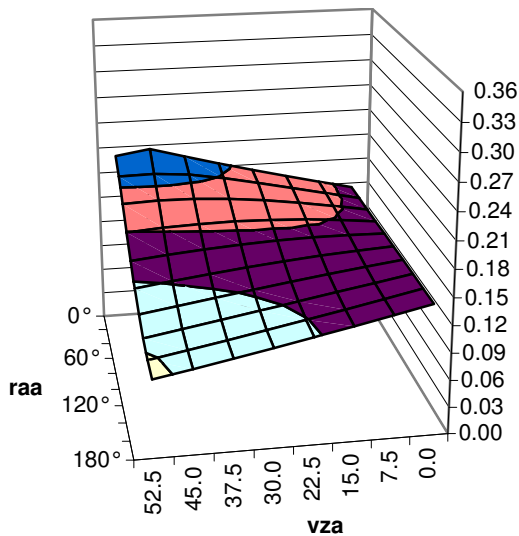


Figure 4: Modelled VIS reflectance for olive grows where  $NDVI = NDVI_{mean} - NDVI_{stddev}$

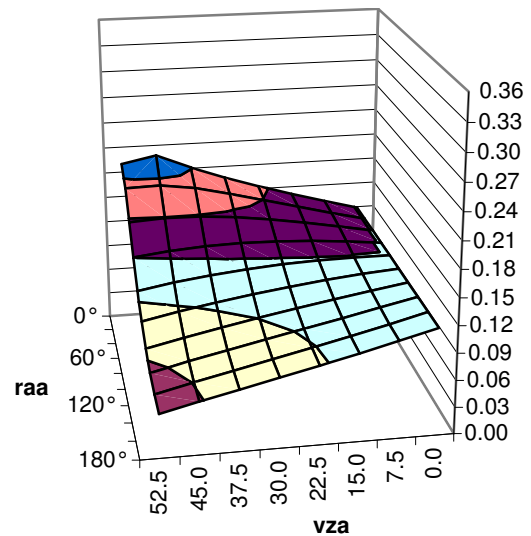


Figure 5: Modelled VIS reflectance for olive grows where  $NDVI = NDVI_{mean} + NDVI_{stddev}$

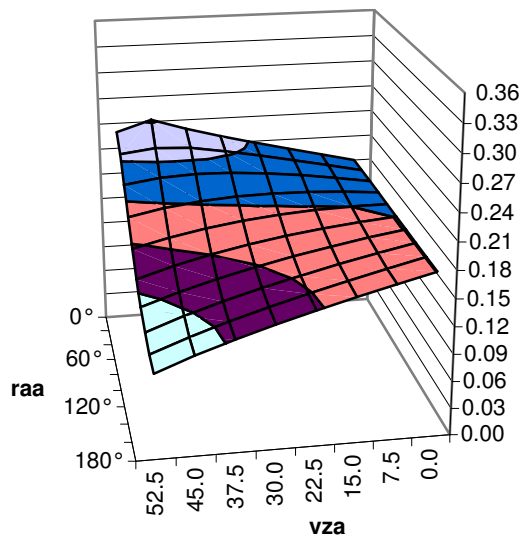


Figure 6: Modelled NIR reflectance for olive groves where  $NIR - VIS = (NIR - VIS)_{mean} - (NIR - VIS)_{stddev}$

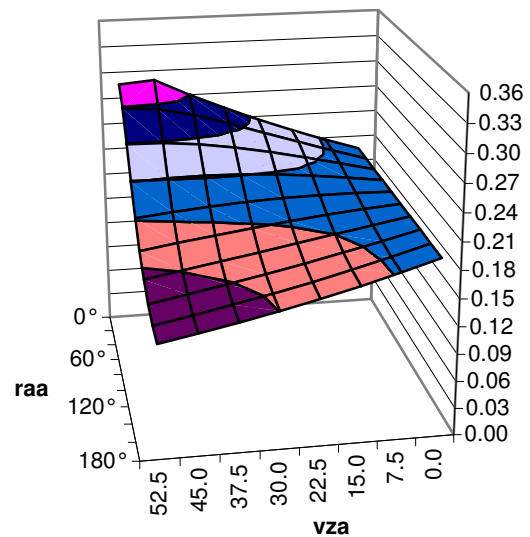


Figure 7: Modelled NIR reflectance for olive groves where  $NIR - VIS = (NIR - VIS)_{mean} + (NIR - VIS)_{stddev}$

#### 4. CONCLUSIONS

It has been shown that the NTAM possesses a big potential to reduce BRDF effects in AVHRR imagery of Spain. This is quantitatively expressed by the good results in model inversion for the two channels and on practically all land cover classes. Apart from the good results, the main advantages of the NTAM are its physical foundations and its simplicity, as only one set of parameters for land cover class and channel has to be provided to correct for the whole vegetation period.

The derived correction parameters offer a great potential for interpretation of land cover specific biophysical properties.

Results of the forward mode of BRDF correction are not discussed in this paper. Future work should address the transition pixel problem which is enhanced in the forward mode of BRDF correction. As landscape in Spain is obviously structured on a larger scale than Canada, the land cover based approach is to be further investigated.

#### REFERENCES

Aguado, I., Chuvieco, E., Martín, P., Salas, F.J. 2003. Assessment of forest fire danger conditions in southern Spain from NOAA images and meteorological indices. *International Journal of Remote Sensing*. 24. 1653 -1668

Chen, J.M., Cihlar, J. 1997. A hotspot function in a simple bidirectional reflectance model for satellite applications. *Journal of Geophysical Research*. 102. 25907-25913

Chuvieco, E. 2002. *Teledetección ambiental*. Ariel Ciencia

Chuvieco, E., Aguado, I., Cocero, D., Riano, D. 2003. Design of an empirical index to estimate fuel moisture content from NOAA-AVHRR analysis in forest fire danger studies. *International Journal of Remote Sensing*. 24. 1621-1637 .

Cihlar, J., Chen, J., Li, Z., Latifovic, R., Fedosejevs, G., Adair, M., Parl, W., Fraser, R., Trishenko, A., Guindon, B., Stanley, D., Morse, D. 2002. GeoComp-n, an advanced system for the processing of coarse and medium resolution satellite data. Part 2: Biophysical products for Northern ecosystems. *Canadian Journal for Remote Sensing*. 28. 21-44

Chopping, M.J. 2000. Large-scale BRDF retrieval over New Mexico with a multiangular NOAA AVHRR dataset. *Remote Sensing of Environment*. 74. 163-191

CORINE Land Cover Report - From land cover to landscape diversity. 2000. DG AGRI, EUROSTAT, the Joint Research Centre (Ispra) and the European Environmental Agency

Cracknell, A. 1997. *The Advanced Very High Resolution Radiometer (AVHRR)*. Taylor and Francis

Dymond, J.R., Shepherd, J.D., Qi, J. 2001. A simple physical model of vegetation for standardising optical satellite imagery. *Remote Sensing of Environment*. 77. 230-239

Hu, B., Lucht, W., Strahler, A.H., Schaaf, C.B., Smith, M. 2000. Surface albedos and angle corrected NDVI from AVHRR observations of South America. *Remote Sensing of Environment*. 71. 119-132

KLM User's Guide. 2000. Edited by: GOODRUM, G., KIDWELL, K.B., WINSTON, W. National Oceanic and Atmospheric Administration. Suitland, MD 20746-4304

Latifovic, R., Cihlar, J., Chen, J. 2003. A comparison of BRDF models for the normalisation of satellite optical data to a standard sun-sensor-target geometry. *IEEE Transactions on Geoscience and Remote Sensing*. 8. 1889-1898

Leroy, M., Roujean, J.L. 1994. Sun and view angle corrections on reflectance derived from NOAA AVHRR data. *IEEE Transactions on Geoscience and Remote Sensing*. 32(3). 684-697

- Ni, W., Li, X., Woodcock, C.E., Caetano, M.R., Strahler, A.H. 1999. An analytical hybrid GORT model for bidirectional reflectance over discontinuous plant canopies. *IEEE Transactions on Geoscience and Remote Sensing*. 37. 987-999.
- Ni, W., Li, X. 2000. A coupled vegetation-soil bidirectional reflectance model for semiarid landscape. *Remote Sensing of Environment*. 74. 113-124
- O'Brien, D.M., Mitchell, R.M., Edwards, M., Ellum, C.C. 1998. Estimation of BRDF from AVHRR short-wave channels: tests over semiarid Australian sites. *Remote Sensing of Environment*. 66. 71-86
- Roujean, J.-L., Leroy, M., Deschamps, P.-Y. 1992. A bidirectional reflectance model of the Earth's surface for the correction of remote sensing data. *Journal of Geophysical Research*. 97 (D18): 20455-20468)
- Sandmeier, S.R., Itten, K.I. 1999. A field goniometer system (FIGOS) for acquisition of hyperspectral BRDF data. *IEEE Transactions on Geoscience and Remote Sensing*. 37. 978-986
- Saunders, R.W., Kriebel, K.T., 1988. An improved method for detecting clear sky and cloudy radiances from AVHRR data. *International Journal for Remote Sensing*. 9. 123-150
- Shepherd, J.D., Dymond, J.R. 2000. BRDF correction of vegetation in AVHRR imagery. *Remote Sensing of Environment*. 74. 397-408
- Walthall, C.L., Norman, J.M., Welles, J.M., Campbell, G., Blad, B.L. 1985. Simple equation to approximate the bidirectional reflectance from vegetative canopies and bare soil surfaces. *Applied Optics*. 24. 383-387
- Wanner, W., Li, X., Strahler, A.H., 1995. On the derivation of kernels for kernel-driven models of bidirectional reflectance. *Journal of Geophysical Research*. 100. 21077-21090

#### **ACKNOWLEDGEMENTS**

I would like to thank those people who contributed to this work with their help and advice. First of all, I owe thanks to Prof. Dr. Emilio Chuvieco and the staff from his institute for utter support and scientific conduct. In addition, I like to thank Rasim Latifovic and Josef Cihlar from the CCRS for providing the model inversion software.